AIChE

Thermophoresis of Axisymmetric Aerosol Particles Along Their Axes of Revolution

Yu C. Chang and Huan J. Keh
Department of Chemical Engineering, National Taiwan University, Taipei, Taiwan 10617, Republic of China

DOI 10.1002/aic.11624
Published online November 21, 2008 in Wiley InterScience (www.interscience.wiley.com).

The axisymmetric thermophoretic motion of an aerosol particle of revolution in a uniformly prescribed temperature gradient is studied theoretically. The Knudsen number is assumed to be small so that the fluid flow is described by a continuum model. A method of distribution of a set of spherical singularities along the axis of revolution within a prolate particle or on the fundamental plane within an oblate particle is used to find the general solutions for the temperature distribution and fluid velocity field. The jump/slip conditions on the particle surface are satisfied by applying a boundary-collocation technique to these general solutions. Numerical results for the thermophoretic velocity of the particle are obtained with good convergence behavior for various cases. For the axisymmetric thermophoresis of an aerosol spheroid with no temperature jump and frictional slip at its surface, the agreement between our results and the available analytical solutions is very good. The thermophoretic velocity of a spheroid along its axis of revolution in general increases with an increase in its axial-to-radial aspect ratio, but there are exceptions. For most practical cases of a spheroid with a specified aspect ratio, its thermophoretic mobility is not a monotonic function of its relative jump/slip coefficients and thermal conductivity. © 2008 American Institute of Chemical Engineers *AIChE J,* 55: 35–48, 2009

Keywords: thermophoresis, axisymmetric aerosol particle, spheroid, temperature jump, thermal and frictional slip

Introduction

A particle, when suspended in a gas possessing a temperature gradient, acquires a velocity relative to the gas in a direction of decreasing temperature. This phenomenon, known as thermophoresis, was first observed by Tyndall in 1870 when it was discovered that a dust-free space surrounded a hot body.[1] Being a mechanism for the capture of aerosol particles on cool surfaces, thermophoresis is of considerable importance in many practical applications. For example, thermophoresis can be effective in removing or collecting small particles from laminar gas streams in air cleaning and aerosol sampling devices.[2,3] The phenomenon has also been cited as an origin for the deposition of particulate matter on surfaces of heat exchangers causing scale formation with the attendant reduction of the heat-transfer coefficient[4] and supporting the development of systems for filterless removal of combustion aerosol particles.[5] Convincing evidence has been provided that, in the modified chemical vapor deposition process for the manufacture of high-quality optical fibers, thermophoresis is the primary mechanism responsible for the deposition of aerosol particles (soot) onto the inner walls of the containing tube.[6,7] On the other hand, deposition of contaminant particles by thermophoresis on wafers in clean rooms during manufacturing steps can be a

Additional Supporting Information may be found in the online version of this article.

Correspondence concerning this article should be addressed to H. J. Keh at huan@ntu.edu.tw.

© 2008 American Institute of Chemical Engineers

major cause of loss of product yields in the microelectronics industry.[8] In the area of nuclear safety, knowledge of thermophoresis is required to calculate the deposition rates of radioactive aerosol particles released in reactor accident situations where large temperature gradients exist.[9]

The thermophoretic effect can be explained in part by appealing to the kinetic theory of gases.[10] The higher-energy gas molecules in the hot regions impinge on the particle with greater momenta than molecules coming from the cold regions, thus resulting in the migration of the particle in the direction of decreasing temperature. Theoretical analyses yield an expression for the thermophoretic velocity of a spherical particle in a constant temperature gradient ∇T_∞ as

$$\mathbf{U} = -M\nabla T_\infty, \tag{1}$$

where the negative sign indicates that the particle motion is in the direction of decreasing temperature. The thermophoretic mobility M depends on the magnitude of the Knudsen number, l/b, where l is the mean free path of the gas molecules and b is a characteristic linear dimension of the particle.

In the regime of small Knudsen number, the fluid flow may be described by a continuum model and the thermophoretic force arises from a thermal slip along the particle surface because of the existence of a tangential temperature gradient at the surface. Utilizing the gas kinetic theory, Maxwell[11] predicted that a tangential temperature gradient $\nabla_s T$ at a gas-solid surface would cause a thin layer of gas (known as the Knudsen layer) adjacent to the surface to move (which can be viewed as a thermo-osmotic flow), with the relative velocity at the outer edge of the layer being

$$\mathbf{v}^{(s)} = C_s \frac{\eta}{\rho_f T} \nabla_s T, \tag{2}$$

where η is the fluid viscosity, ρ_f is the fluid density, and T is the local gas temperature. The thermal slip coefficient C_s was found to be 3/4 by Maxwell on the assumption that the distribution function in the bulk of the gas held all the way to the solid wall. Note that the thermal slip velocity $\mathbf{v}^{(s)}$ is directed toward the high temperature side and $\rho_f T$ in Eq. 2 is a constant for an ideal gas at constant pressure.

By using the Maxwellian slip velocity in Eq. 2, which gives the coupling between temperature and velocity fields, as a slip-velocity boundary condition and solving the equation of continuum fluid motion incorporating with the heat conduction in the gas and particle at low Reynolds and Peclet numbers, Epstein[12] derived an expression for the thermophoretic mobility of a suspended aerosol sphere as

$$M = \frac{2C_s \eta k}{\rho_f T_0 (2k + k_1)}, \tag{3}$$

where k and k_1 are thermal conductivities of the gas and particle, respectively, and T_0 is the bulk-gas absolute temperature at the particle center in the absence of the particle (or the mean gas temperature in the vicinity of the particle). The thermophoretic velocity predicted by Eqs. 1 and 3, which is independent of particle size, is in fair agreement with experimental data when the ratio k_1/k is not too high.

The solution for the thermophoretic velocity obtained by Epstein was improved by Brock[13] using the low-Knudsen-number effects of the temperature jump at the gas-particle surface as well as the frictional (isothermal) gas slippage (in addition to the thermal slip) along the surface. The resulting expression for the thermophoretic mobility of an aerosol sphere of radius b is

$$M = \frac{2C_s \eta (k + k_1 C_t l/b)}{\rho_f T_0 (1 + 2C_m l/b)(2k + k_1 + 2k_1 C_t l/b)}, \tag{4}$$

where the dimensionless coefficients C_t and C_m (numerical factors of order unity) account for the temperature jump and frictional slip, respectively, at the particle surface and must be determined experimentally for each gas-solid system. Note that Eq. 4 is applicable to the range of finite Knudsen number and reduces to Eq. 3 when $l/b = 0$.

Satisfactory agreement of the prediction by Eq. 4 with experiments[14,15] has been obtained. Derjaguin et al.[16,17] presented the experimental data of the thermophoretic mobility for a variety of aerosols, which are in good agreement with Eq. 4 with $C_m = 0$, $C_s = 3/2$ and a suitable selection of the coefficient C_t. A set of kinetic-theory values for complete thermal and momentum accommodations appear to be $C_s = 1.17$, $C_t = 2.18$ and $C_m = 1.14$.[18] Recently, kinetic-theory values of these slip coefficients have been obtained accurately under various conditions.[19–22] According to Eq. 4, particles with large thermal conductivity and small Knudsen number (say, $k_1/k = 100$ and $l/b = 0.01$) will migrate by thermophoresis at velocities of 10–50 μm s^{-1} in temperature gradients of order 100 K cm^{-1} such gradients are easily attainable in thermal boundary layers.

Most aerosol particles are not spherical[23,24] and it is therefore of considerable interest to examine the effect of particle shape on thermophoresis. The thermophoretic theories of nonspherical particles differ from those of spheres in that there is an orientational problem. In general, the thermophoretic mobility of a nonspherical particle is anisotropic and the velocity of the particle is no longer collinear with the prescribed temperature gradient. The thermophoretic motion of a long circular cylinder in the direction normal to its axis has been studied with the consideration of the effects of temperature jump, thermal slip, and frictional slip at the particle surface.[25,26] On the other hand, the axisymmetric thermophoresis of a spheroidal particle along its axis of revolution without temperature jump and frictional slip at its surface was also analyzed.[27,28] This analysis has been generalized to a spheroid with an arbitrary orientation relative to the thermal gradient.[29] Recently, the thermophoresis of a particle which departs slightly in shape from a sphere with the effects of temperature jump, thermal slip and frictional slip was investigated, and an explicit expression for the thermophoretic velocity was obtained to the first order in the small parameter characterizing the deformation.[30] However, the problem of thermophoresis of particles of a general shape with all the effects of temperature jump, thermal slip, and frictional slip at the particle surface has not been solved yet, mainly due to the fact that, if the temperature jump and/or frictional slip is included, a separable solution is not feasible for most orthogonal curvilinear coordinate systems, such as the prolate and oblate spheroidal ones.[27–29]

In this article we use a method of distributed internal singularities incorporated with a boundary-collocation technique to analyze the thermophoretic motion of an arbitrary particle of revolution along its axis of symmetry; the particle can be either prolate or oblate. The thermophoretic velocity of the particle as a function of the physical and surface properties of the particle-gas system is calculated for various cases. For the special cases of a sphere in general conditions and of a spheroid with no temperature jump and frictional slip, our results of the thermophoretic velocity show excellent agreement with the exact solutions.[13,27–29] For the cases of a spheroid in general conditions whose shape deviates slightly from that of a sphere, our results also agree quite well with the approximate analytical solution in the literature.[30]

Mathematical Description of the Thermophoresis Problem

We consider the steady thermophoresis of a general axisymmetric rigid particle in an unbounded gaseous medium along its axis of revolution, as shown in Figure 1. Here (ρ,ϕ,z) and (r,θ,ϕ) denote the circular cylindrical and spherical coordinate systems, respectively, and the origin of coordinates is chosen at the particle center. A linear temperature field $T_\infty(z)$ with a uniform thermal gradient $-E_\infty \mathbf{e}_z$ $(= \bigtriangledown T_\infty)$ is imposed in the ambient fluid far removed from the particle, where $\mathbf{e}_z$ is the unit vector in the z direction and, for convenience, E_∞ is taken to be positive. It is assumed that the Knudsen number l/b is small so that the fluid flow is in the continuum regime and the Knudsen layer at the particle surface is thin in comparison with the linear dimensions of the particle.

To determine the velocity of the particle undergoing axially symmetric thermophoretic motion, it is necessary to ascertain the temperature distributions inside and outside the particle and the velocity field in the fluid phase.

Temperature distributions

For the heat transfer in a system of thermophoresis, the Peclet number can be assumed to be small. Hence, the energy equations governing the temperature distributions are

$$\nabla^2 T = 0 \quad \text{and} \quad \nabla^2 T_1 = 0 \tag{5}$$

for the fluid and particle, respectively.

The boundary conditions at the particle surface require that the normal component of heat flux be continuous and a temperature jump that is proportional to the normal temperature gradient[10,13] occur. Also, the fluid temperature far away from the particle approaches the undisturbed quantities. Thus, we can write

$$\left.\begin{aligned} k\mathbf{n}\cdot\nabla T &= k_1 \mathbf{n}\cdot\nabla T_1 \\ T - T_1 &= C_t l \mathbf{n}\cdot\nabla T \end{aligned}\right\} \quad \text{on } S_p, \tag{6a}$$

and

$$T \to T_\infty = T_0 - E_\infty z \quad \text{as } r \to \infty. \tag{6b}$$

Here, $\mathbf{n}$ is the unit normal vector at the particle surface S_p pointing into the fluid, k and k_1 are the thermal conductivities of the fluid and particle, respectively, and C_t is the temperature jump coefficient about the surface of the particle; k, k_1, and C_t are assumed to be constant. At the temperature range of 300–400 K, $k_1 = 0.022$–0.024 W m^{-1} K^{-1} for silica aerosol and $k_1 = 0.9$–3 W m^{-1} K^{-1} for clay, soil, and stone, whereas $k = 0.026$–0.033 W m^{-1} K^{-1} for air.[31]

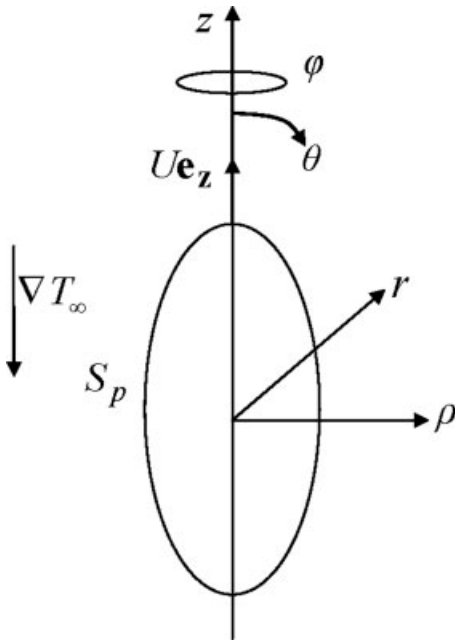

Figure 1. Geometrical sketch for the thermophoresis of an arbitrary axisymmetric particle along its axis of revolution.

To solve Eqs. 5 and 6, a set of spherical singularities is chosen and distributed along the axis of revolution within a prolate particle or on the fundamental plane within an oblate particle.[32,33] The temperature distributions inside and outside the particle are approximated by the superposition of the set of the spherical singularities and the boundary conditions in Eq. 6a on the particle surface can be satisfied by making use of the multipole collocation method. For the special case of a spherical particle, only a single singularity which is placed at the particle center is needed.

The temperature distributions external and internal to the particle caused by a spherical singularity at the point $\rho = 0$ and $z = h$ are

$$T = T_0 - E_\infty z + E_\infty \sum_{n=0}^{\infty} [H_n L_{1n}(\rho, z-h)], \tag{7a}$$

and

$$T_1 = T_0 + E_\infty \sum_{n=0}^{\infty} [\overline{H}_n L_{2n}(\rho, z-h)], \tag{7b}$$

respectively, where L_{in} with $i = 1$ and 2 are functions of position defined by Eq. A1 in the Supporting Information section, and H_n and $\overline{H}_n$ are unknown constant coefficients. Note that the boundary condition 6b is immediately satisfied by a solution in the form of Eq. 7a.

In circular cylindrical coordinates, the boundary condition 6a on the particle surface for the axisymmetric temperature field can be expressed as

$$\left.\begin{array}{l} k(n_\rho E_\rho + n_z E_z) = k_1(n_\rho E_{1\rho} + n_z E_{1z}) \\ T - T_1 = C_t l(n_\rho E_\rho + n_z E_z) \end{array}\right\} \quad \text{on } S_p. \tag{8}$$

In this equation, n_ρ and n_z are the local ρ and z components of the unit normal vector $\mathbf{n}$, and E_ρ, $E_{1\rho}$, E_z, and E_{1z} are the components of the local temperature gradients inside and outside the particle, which can be obtained form Eqs. 7a and 7b as

$$E_\rho = \frac{\partial T}{\partial \rho} = E_\infty \sum_{n=0}^{\infty} [H_n \delta_{1n}(\rho, z-h)], \tag{9a}$$

$$E_{1\rho} = \frac{\partial T_1}{\partial \rho} = E_\infty \sum_{n=0}^{\infty} [\overline{H}_n \delta_{2n}(\rho, z-h)], \tag{9b}$$

$$E_z = \frac{\partial T}{\partial z} = -E_\infty + E_\infty \sum_{n=0}^{\infty} [H_n \varepsilon_{1n}(\rho, z-h)], \tag{9c}$$

$$E_{1z} = \frac{\partial T_1}{\partial z} = E_\infty \sum_{n=0}^{\infty} [\overline{H}_n \varepsilon_{2n}(\rho, z-h)], \tag{9d}$$

where δ_{in} and ε_{in} with $i = 1$ and 2 are functions of position defined by Eq. A2.

Fluid velocity distribution

With knowledge of the solution for the external temperature distribution on the particle surface which drives the thermophoretic migration, we now proceed to find the flow field. Owing to the low Reynolds number encountered in thermophoresis, the fluid motion is governed by the Stokes equations,

$$\eta \nabla^2 \mathbf{v} - \nabla p = \mathbf{0}, \quad \nabla \cdot \mathbf{v} = 0, \tag{10}$$

where $\mathbf{v}$ is the fluid velocity field and p is the dynamic pressure distribution.

There exist thermal and frictional slip velocities along the particle surface and the fluid flow vanishes far from the particle. Hence, the boundary conditions for the fluid velocity are[13,34]

$$\mathbf{v} = U\mathbf{e}_z + \frac{C_m l}{\eta}(\mathbf{I} - \mathbf{nn})\mathbf{n} : \tau + \frac{C_s \eta}{\rho_f T_0}(\mathbf{I} - \mathbf{nn}) \cdot \nabla T \quad \text{on } S_p, \tag{11a}$$

$$\mathbf{v} \to \mathbf{0} \quad \text{as } r \to \infty. \tag{11b}$$

Here, $\tau (= \eta[\nabla \mathbf{v} + (\nabla \mathbf{v})^T])$ is the viscous stress tensor, $\mathbf{I}$ is the unit dyadic, C_s is the thermal slip coefficient defined in Eq. 2, C_m is the frictional slip coefficient, and U is the thermophoretic velocity of the particle to be determined. The tangential temperature gradient in Eq. 11a can be obtained from Eqs. 9a and 9c.

Analogous to the solution procedure for the temperature field presented in the previous subsection, Eqs. 10 and 11 can be solved by distributing a set of Sampson spherical singularities (also called Sampsonlets) along the axis of revolution within a prolate particle or on the fundamental plane within an oblate particle.[32,33] The flow field surrounding the particle is approximated by the superposition of the set of the spherical singularities and the boundary condition 11a on the particle surface is satisfied by using the multipole collocation method.

The velocity components for the axisymmetric fluid motion caused by a Sampson spherical singularity at the point $\rho = 0$ and $z = h$ are[35,36]

$$v_\rho = \sum_{n=2}^{\infty} [B_n A_{1n}(\rho, z-h) + D_n A_{2n}(\rho, z-h)], \tag{12a}$$

$$v_z = \sum_{n=2}^{\infty} [B_n C_{1n}(\rho, z-h) + D_n C_{2n}(\rho, z-h)], \tag{12b}$$

and $v_\phi = 0$, where A_{in} and C_{in} with $i = 1$ and 2 are functions of position defined by Eq. A3 in the Supporting Information section, and B_n and D_n are unknown constant coefficients. Note that the boundary condition 11b is immediately satisfied by a solution in the form of Eq. 12.

In cylindrical coordinates, the boundary condition 11a on the particle surface for the axisymmetric flow can be expressed as

$$\left.\begin{array}{l} v_\rho = \dfrac{C_m l}{\eta}[(1-n_\rho^2)n_\rho \tau_{\rho\rho} - n_\rho n_z^2 \tau_{zz} + (1-2n_\rho^2)n_z \tau_{\rho z}] \\ \qquad + \dfrac{C_s \eta}{\rho_f T_0}[(1-n_\rho^2)E_\rho - n_z n_\rho E_z] \\ v_z = U + \dfrac{C_m l}{\eta}[(1-n_z^2)n_z \tau_{zz} - n_z n_\rho^2 \tau_{\rho\rho} + (1-2n_z^2)n_\rho \tau_{\rho z}] \\ \qquad + \dfrac{C_s \eta}{\rho_f T_0}[(1-n_z^2)E_z - n_z n_\rho E_\rho] \end{array}\right\} \quad \text{on } S_p. \tag{13}$$

From Eq. 12, the components of the viscous stress tensor in Eq. 13 can be obtained as

$$\tau_{\rho\rho} = \eta \sum_{n=2}^{\infty} [B_n \alpha_{1n}(\rho, z-h) + D_n \alpha_{2n}(\rho, z-h)], \tag{14a}$$

$$\tau_{zz} = \eta \sum_{n=2}^{\infty} [B_n \beta_{1n}(\rho, z-h) + D_n \beta_{2n}(\rho, z-h)], \tag{14b}$$

$$\tau_{\rho z} = \eta \sum_{n=2}^{\infty} [B_n \gamma_{1n}(\rho, z-h) + D_n \gamma_{2n}(\rho, z-h)], \tag{14c}$$

where α_{in}, β_{in}, and γ_{in} with $i = 1$ and 2 are functions of position defined by Eq. A4.

The drag force exerted by the fluid on the surface of the particle caused by the Sampson spherical singularity can be determined from

$$F = 4\pi\eta D_2. \tag{15}$$

That is, only the first multipole of the spherical singularity contributes to the hydrodynamic drag on the particle.

Equations 7 and 9 for temperature fields, Eqs. 12 and 14 for the fluid flow fields, and Eq. 15 for the hydrodynamic drag force caused by a Sampsonlet as well as boundary conditions 8 and 13 on the particle surface will be utilized in the following sections to solve for the thermophoretic velocity of a particle of revolution along its axis of symmetry.

Solution for the Thermophoresis of a Spherical Particle

In this section, a spherical singularity described in the previous section is used with the boundary collocation technique to obtain the numerical solution for the thermophoretic motion of a spherical particle of radius b. The collocation result of the thermophoretic velocity will be compared with the exact analytical solution given by Eqs. 1 and 4.

Temperature distributions

The temperature field inside and outside the spherical particle produced by the imposed thermal gradient can be represented by a spherical singularity placed at its center which is the origin of the coordinate frame. Thus, the distributions of the temperature and the components of its gradients for the heat conduction around the sphere are given by Eqs. 7 and 9 with $h = 0$. To determine the unknown constants H_n and $\overline{H}_n$, one can apply the boundary conditions in Eq. 8 at the particle surface to these distributions to yield

$$\left.\begin{aligned}\sum_{n=0}^{\infty}\left[H_n M_{1n}^{*}(\rho,z)+\overline{H}_n M_{2n}^{*}(\rho,z)\right]&=n_z\\ \sum_{n=0}^{\infty}\left[H_n M_{1n}^{**}(\rho,z)+\overline{H}_n M_{2n}^{**}(\rho,z)\right]&=z-C_{\mathrm{t}}^{*}bn_z\end{aligned}\right\}\quad \text{at } r=b, \tag{16}$$

where

$$M_{1n}^{*}(\rho,z)=n_\rho\delta_{1n}(\rho,z)+n_z\varepsilon_{1n}(\rho,z), \tag{17a}$$

$$M_{2n}^{*}(\rho,z)=-k^{*}[n_\rho\delta_{2n}(\rho,z)+n_z\varepsilon_{2n}(\rho,z)], \tag{17b}$$

$$M_{1n}^{**}(\rho,z)=L_{1n}(\rho,z)-C_{\mathrm{t}}^{*}bM_{1n}^{*}(\rho,z), \tag{17c}$$

$$M_{2n}^{**}(\rho,z)=-L_{2n}(\rho,z), \tag{17d}$$

$$k^{*}=k_1/k \text{ and } C_{\mathrm{t}}^{*}=C_{\mathrm{t}}l/b.$$

To satisfy the boundary condition 16 exactly along the entire semicircular generating arc of the sphere in a meridian plane would require the solution of the entire infinite array of the unknown constants H_n and $\overline{H}_n$. However, the boundary-collocation technique[37–40] enforces the boundary condition at a finite number of discrete points on the particle's generating arc and truncates the infinite series in Eqs. 7, 9, and 16 into finite ones. The unknown constants in each term of the series permit one to satisfy the exact boundary conditions at one discrete point on the particle surface. Thus, if the boundary is approximated by satisfying condition 16 at N_{T} discrete points (values of θ between 0 and π), then the infinite series are truncated after N_{T} terms, resulting in a system of $2N_{\mathrm{T}}$ simultaneous linear algebraic equations in the truncated form of Eq. 16. This matrix equation can be solved by any of the standard matrix-reduction techniques to yield the $2N_{\mathrm{T}}$ unknown constants H_n and $\overline{H}_n$ required in the truncated equations for the temperature field. The accuracy of the truncation technique can be improved to any degree by taking a sufficiently large value of N_{T}. Naturally, the truncation error vanishes as $N_{\mathrm{T}} \to \infty$.

Fluid velocity distribution

The fluid flow accompanying the thermophoresis of a spherical particle can be represented by a Sampsonlet placed at its center. Thus, the velocity and stress components for the fluid motion are given by Eqs. 12 and 14 with $h = 0$. To determine the unknown constants B_n and D_n, one can apply the boundary conditions in Eq. 13 at the particle surface to these velocity and stress components to yield

$$\left.\begin{aligned}\sum_{n=2}^{\infty}\left[B_n A_{1n}^{*}(\rho,z)+D_n A_{2n}^{*}(\rho,z)\right]&\\ =C_{\mathrm{s}}\frac{\eta E_\infty}{\rho_{\mathrm{f}}T_0}\left[n_z n_\rho+\sum_{n=0}^{\infty}H_n\delta_{1n}^{*}(\rho,z)\right]&\\ \sum_{n=2}^{\infty}\left[B_n C_{1n}^{*}(\rho,z)+D_n C_{2n}^{*}(\rho,z)\right]&\\ =U+C_{\mathrm{s}}\frac{\eta E_\infty}{\rho_{\mathrm{f}}T_0}\left[(n_z^2-1)+\sum_{n=0}^{\infty}H_n\varepsilon_{1n}^{*}(\rho,z)\right]&\end{aligned}\right\}\quad \text{at } r=b, \tag{18}$$

where

$$\delta_{1n}^{*}(\rho,z)=(1-n_\rho^2)\delta_{1n}(\rho,z)-n_z n_\rho\varepsilon_{1n}(\rho,z), \tag{19a}$$

$$\varepsilon_{1n}^{*}(\rho,z)=(1-n_z^2)\varepsilon_{1n}(\rho,z)-n_z n_\rho\delta_{1n}(\rho,z), \tag{19b}$$

$$\begin{aligned}A_{in}^{*}(\rho,z)\ =&A_{in}(\rho,z)-C_{\mathrm{m}}^{*}b[(1-n_\rho^2)n_\rho\alpha_{in}(\rho,z)\\ &-n_\rho n_z^2\beta_{in}(\rho,z)\ +(1-2n_\rho^2)n_z\gamma_{in}(\rho,z)],\end{aligned} \tag{19c}$$

$$\begin{aligned}C_{in}^{*}(\rho,z)\ =&C_{in}(\rho,z)-C_{\mathrm{m}}^{*}b[(1-n_z^2)n_z\beta_{in}(\rho,z)\\ &-n_z n_\rho^2\alpha_{in}(\rho,z)\ \ +(1-2n_z^2)n_\rho\gamma_{in}(\rho,z)],\end{aligned} \tag{19d}$$

$C_{\mathrm{m}}^{*} = C_{\mathrm{m}}l/b$ and $i = 1$ or 2. The first N_{T} coefficients H_n have been determined through the procedure given in the previous subsection.

Equation 18 can be satisfied by utilizing the boundary collocation technique presented for the solution of the temperature field. Along a longitudinal generating arc at the particle surface, Eq. 18 is applied at N_{H} discrete points (values of θ between 0 and π) and the infinite series in Eqs. 12 and 14 are truncated after N_{H} terms. This generates a set of $2N_{\mathrm{H}}$ linear algebraic equations for the $2N_{\mathrm{H}}$ unknown coefficients B_n and D_n. The fluid velocity field is completely obtained once these coefficients are solved for a sufficiently large number of N_{H}.

Thermophoretic velocity of the particle

Because the particle is freely suspended in the surrounding fluid, the net force acting on the particle must vanish. Applying this constraint to Eq. 15, one obtains

Table 1. Numerical Results of the Dimensionless Thermophoretic Velocity of a Sphere with $C_t^* = 2C_m^*$ for Various Values of the Parameters k^* and C_m^*

k^*	C_m^*	$N_T = N_H$	$U\rho_f T_0/C_s\eta E_\infty$
100	0	4	0.0196
		8	0.0196
		Exact solution	0.0196
100	0.1	4	0.2465
		8	0.2465
		Exact solution	0.2465
1	0.1	4	0.5882
		8	0.5882
		Exact solution	0.5882

Exact solutions are calculated from Eqs. 1 and 4.

$$D_2 = 0. \tag{20}$$

To determine the thermophoretic velocity U of the particle, Eq. 20 and the $2N_H$ algebraic equations resulting from Eq. 18 are to be solved simultaneously.

When specifying the points along the semicircular generating arc of the sphere where the boundary conditions are exactly satisfied, the first point that should be chosen is $\theta = \pi/2$, because this point defines the projected area of the particle normal to the direction of motion. In addition, the points $\theta = 0$ and $\theta = \pi$ are also important. However, an examination of the systems of linear algebraic equations 16 and 18 shows that the coefficient matrices become singular if these points are used. To overcome the difficulty of singularity and to preserve the geometric symmetry of the particle surface about the equatorial plane $\theta = \pi/2$, points at $\theta = \alpha$, $\pi/2 - \alpha$, $\pi/2 + \alpha$ and $\pi - \alpha$ are taken to be four basic collocation points.[33,38,39] Additional points along the boundary are usually selected as mirror-image pairs about the plane $\theta = \pi/2$ to divide the θ coordinate into equal parts. The optimum value of α in this work is found to be 0.01°, with which the numerical results of the thermophoretic velocity of the particle can converge to at least four significant figures. In principle, as long as the number of the collocation points is sufficiently large and the distribution of the collocation points is adequate, the solution of the particle velocity will converge and the shape of the particle can be well approximated, irrespective of the particle shape or boundary conditions.

In our continuum-with-slippage analysis given in the previous section, the Knudsen number (l/b) of the system should be smaller than about 0.1. As mentioned in the first section, a set of well adapted values for the temperature jump and frictional slip coefficients under the condition of complete energy and momentum accommodations are 2.18 and 1.14, respectively. Consequently, the normalized coefficients C_t^* and C_m^* must be restricted to be less than unity. For convenience we will use the ratio $C_t^*/C_m^* = 2$ (a rounded value to $2.18/1.14 = 1.91$) throughout the article, without the loss of reality or generality. On the other hand, the thermal conductivity of an aerosol particle is usually greater than that of the ambient gas. Thus, the value of the relative conductivity k^* will exceed unity under most practical situations.

In Table 1, a number of numerical solutions of the dimensionless thermophoretic velocity $U\rho_f T_0/C_s\eta E_\infty$ of the aerosol sphere are presented for various values of the parameters C_m^* ($=C_t^*/2$) and k^* using the boundary collocation technique. All of the results were obtained by increasing the numbers of collocation points N_T and N_H until the convergence of four significant digits is achieved. The exact solutions for $U\rho_f T_0/C_s\eta E_\infty$ calculated using Eqs. 1 and 4 are also listed in Table 1 for comparison. It can be seen that the results from the collocation method agree excellently with the exact results for the desired accuracy and the rate of convergence is rapid.

Axisymmetric Thermophoresis of Prolate Particles

We consider in this section the thermophoretic motion of a general prolate axisymmetric particle along its axis of symmetry. A segment between points A($\rho = 0$, $z = -c_1$) and B($\rho = 0$, $z = c_2$) is taken along the axis of revolution inside the particle on which a set of spherical singularities are distributed (c_1 and c_2 are positive constants). If the nose and tail of the particle are round, then their centers of curvature can be chosen as A and B. The general solutions of the temperature and fluid velocity fields can be constructed by the superposition of the spherical singularities distributed on the segment AB, and Eqs. 7 and 12 are used to result in

$$\begin{bmatrix} T \\ T_1 \end{bmatrix} = \begin{bmatrix} T_0 - E_\infty z \\ T_0 \end{bmatrix} + E_\infty \sum_{n=0}^{\infty} \int_{-c_1}^{c_2} \begin{bmatrix} H_n(t) L_{1n}(\rho, z-t) \\ \overline{H}_n(t) L_{2n}(\rho, z-t) \end{bmatrix} \mathrm{d}t, \tag{21}$$

$$\begin{bmatrix} v_\rho \\ v_z \end{bmatrix} = \sum_{n=2}^{\infty} \int_{-c_1}^{c_2} \left\{ B_n(t) \begin{bmatrix} A_{1n}(\rho, z-t) \\ C_{1n}(\rho, z-t) \end{bmatrix} + D_n(t) \begin{bmatrix} A_{2n}(\rho, z-t) \\ C_{2n}(\rho, z-t) \end{bmatrix} \right\} \mathrm{d}t. \tag{22}$$

The corresponding expressions for the components of the temperature gradient and viscous stress tensor can be obtained using Eqs. 9 and 14.

Equations 21 and 22 provide exact solutions for Eqs. 5 and 10 that satisfy Eqs. 6b and 11b, and the unknown density distribution functions for the singularities, $H_n(t)$, $\overline{H}_n(t)$, $B_n(t)$, and $D_n(t)$, must be determined from the remaining boundary conditions 6a or 8 and 11a or 13 using the collocation technique. From Eqs. 15 and 22, the drag force exerted by the fluid on the prolate particle can be expressed as

$$F = 4\pi\eta \int_{-c_1}^{c_2} D_2(t)\mathrm{d}t. \tag{23}$$

The density distribution functions $H_n(t)$, $\overline{H}_n(t)$, $B_n(t)$, and $D_n(t)$ in Eqs. 21 and 22 can be approximated to various orders of precision to satisfy the boundary conditions at the particle surface. In this work, we consider the constant-distribution, linear-distribution, and quadratic-distribution approximations and their details incorporated with the boundary collocation technique to determine the thermophoretic velocity U of the particle are presented in the Supporting Information section. Note that, similar to the thermophoretic velocity of an aerosol sphere given by Eqs. 1 and 4, the value of U is proportional to the quantity $C_s\eta E_\infty/\rho_f T_0$ and dependent on the dimensionless parameters k^*, C_t^*, and C_m^* (in addition to the aspect ratios of the particle).

Table 2. Numerical Results of the Normalized Thermophoretic Velocity of a Prolate Spheroid with $C_t^* = 2C_m^*$ Along Its Axis of Revolution for Various Values of the Aspect Ratio a/b and the Parameters k^* and C_m^*

a/b	k^*	C_m^*	$N_T = N_H$	M_T	M_H	U/U_0
1.1	100	0	3	4	4	1.1192
					5	1.1192
				6	4	1.1192
			Exact solution			1.1192
1.1	100	0.1	3	17	13	1.0125
					14	1.0127
					15	1.0127
				18	11	1.0127
			Approximate solution			1.0139
1.1	1	0.1	3	16	7	1.0488
					8	1.0489
					9	1.0489
				17	13	1.0489
			Approximate solution			1.0518
2	100	0	4	6	4	2.3180
					5	2.3180
				7	4	2.3180
			Exact solution			2.3180
2	100	0.1	4	37	20	1.0913
					21	1.0911
					22	1.0911
				38	22	1.0911
			Approximate solution			1.1394
2	1	0.1	4	34	21	1.3209
					22	1.3208
					23	1.3208
				35	22	1.3208
			Approximate solution			1.5176

Exact and approximate solutions are calculated from Eqs. 25 and 26, respectively.

Solution for the Thermophoresis of a Prolate Spheroidal Particle

In this section the method presented in the previous section is used to obtain the solution for the axisymmetric thermophoresis of a prolate spheroid. The surface of a spheroid is represented in circular cylindrical coordinates by

$$z(\rho) = \pm a\left[1 - \left(\frac{\rho}{b}\right)^2\right]^{1/2}, \tag{24}$$

where $0 \le \rho \le b$. For the case of a prolate spheroid, a and b are the major and minor semi-axes, respectively ($a > b > 0$).

When the temperature jump and frictional slip do not occur on the surface of the particle (namely, $C_t^* = C_m^* = 0$), the problem of the thermophoresis of a spheroidal particle in a uniform temperature gradient is solvable in the spheroidal coordinate systems by a method of separation of variables. The result for the particle velocity along its axis of revolution is[27–29]

$$U = C_s \frac{\eta E_\infty}{\rho_f T_0} \frac{\zeta[\zeta - (\zeta^2 - 1)\coth^{-1}\zeta]}{k^*(\zeta^2 - 1)(\zeta\coth^{-1}\zeta - 1) + \zeta[\zeta - (\zeta^2 - 1)\coth^{-1}\zeta]}. \tag{25}$$

where $\zeta = a/c$ and $c = (a^2 - b^2)^{1/2}$, which is the half distance between the two foci of the prolate spheroid. In the limit of $a/b \to 1$ or $\zeta \to \infty$, Eq. 25 reduces to Eqs. 1 and 3 for an aerosol sphere.

In a previous section, collocation solutions for the thermophoretic velocity of a spherical particle were presented and shown to be in perfect agreement with the exact solution. We now use the same collocation scheme incorporated with the method of distribution of spherical singularities to obtain the corresponding solution for a prolate spheroid. In Table 2, numerical results of the thermophoretic velocity U of a prolate spheroid with $C_t^* = 2C_m^*$ along its axis of revolution normalized by the corresponding velocity of a sphere, U_0, given by Eqs. 1 and 4 are presented for various values of the aspect ratio a/b and the parameters k^* and C_m^*. The values of U/U_0 are computed by applying either the linear (for $a/b = 1.1$) or the quadratic (for $a/b = 2$) density distribution at each segment. For a spheroid with its aspect ratio close to unity, a constant density distribution of spherical singularities can usually achieve good convergence behavior for the calculation of U. However, when the aspect ratio of the spheroid deviates further from unity, the convergence of the constant density approximation becomes poorer and higher-order approximations should be adopted. The exact solution of U/U_0 for the axisymmetric thermophoresis of a prolate spheroid with no temperature jump and frictional slip ($C_t^* = C_m^* = 0$) calculated using Eq. 25 is also given in Table 2 for comparison. It can be seen that our results from the method of distributed spherical singularities agree very well with the exact solution in this limit. In general, the convergence behavior of the method of spherical singularities is quite good, except for the case of relatively large aspect ratio.

Recently, Senchenko and Keh[30] investigated the problem of thermophoresis of an aerosol particle with a temperature jump, a thermal slip and a frictional slip at the surface whose shape deviates slightly from that of a sphere. Their analytical result for the thermophoretic velocity of a spheroidal particle along its axis of revolution, which is correct to the first order in the small parameter ε characterizing the deformation, can be expressed as

$$U = C_s \frac{\eta E_\infty}{\rho_f T_0}\left\{\frac{2(1 + k^* C_t^*)}{(1 + 2C_m^*)(2 + k^* + 2k^* C_t^*)} - \frac{2}{5}\frac{k^*(6 - k^* C_t^*) + 2C_m^*[14 + k^*(13 + 28C_t^*) + 2k^{*2} C_t^*(3 + 7C_t^*)]}{(1 + 2C_m^*)^2(2 + k^* + 2k^* C_t^*)^2}\varepsilon\right\}, \tag{26}$$

where $\varepsilon = 1 - (a/b)$. When $\varepsilon = 0$, Eq. 26 is identical to Eqs. 1 and 4. The values of the normalized thermophoretic mobility U/U_0 calculated from this approximate formula with $\varepsilon < 0$ are also listed in Table 2 for comparison. It can be found that the solution correct to the first order in ε given by Eq. 26 agrees quite well with our collocation solutions for small magnitudes of ε. The errors are less than 0.3% for particles with $1 \le a/b \le 1.1$. However, the accuracy of this approximate solution begins to deteriorate, as expected, when the value of a/b becomes greater.

The numerical solutions for the normalized thermophoretic velocity U/U_0 of a prolate spheroid with $C_t^* = 2C_m^*$ along its

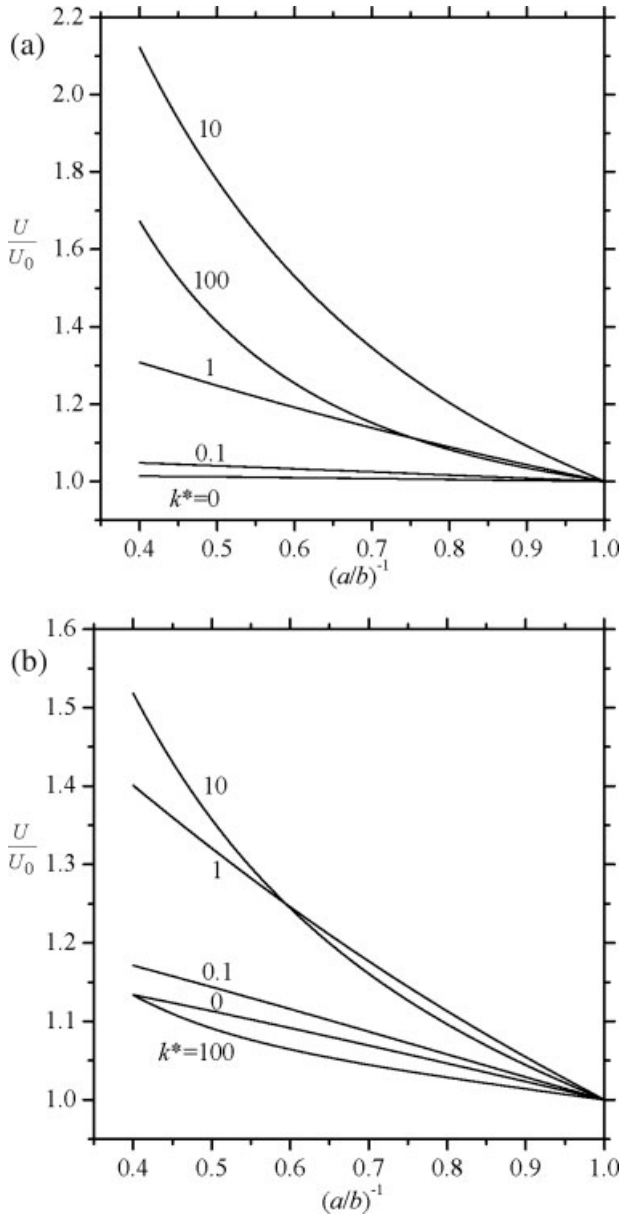

Figure 2. Plots of the normalized thermophoretic velocity U/U_0 of a prolate spheroidal particle along its axis of revolution vs. its aspect ratio $(a/b)^{-1}$ for various values of its relative conductivity k^*: (a) with $C_t^* = 2C_m^* = 0.02$; (b) with $C_t^* = 2C_m^* = 0.2$.

axis of revolution are plotted vs. the aspect ratio a/b, the thermal conductivity ratio k^*, and the slip parameter C_m^* (proportional to the Knudsen number l/b) in Figures 2–4, respectively. The cases of $k^* < 1$, which are not likely to exist in practice, are considered here for the sake of numerical comparison. For specified values of k^*, C_t^*, and C_m^*, the value of U/U_0 in general increases with an increase in a/b, consistent with the trend predicted from Eq. 25 for the limiting case of $C_t^* = C_m^* = 0$. This behavior is understandable because the fraction of the thermal slip of the fluid at the particle surface in the axial direction, which drives the movement of the particle, increases with the increase of a/b. Therefore, the spherical approximation underestimates the axisymmetric thermophoretic mobility for prolate spheroids. When k^* is small (say, <1), U/U_0 decreases almost linearly with an increase in $(a/b)^{-1}$.

For given finite values of C_t^*, C_m^*, and a/b, the value of U/U_0 increases with an increase in k^* when k^* is small, reaches a maximum at some moderate value of k^*, and then decreases with a further increase in k^*, as displayed in Figure 3. This maximum occurs at a higher value of k^* if the value of C_t^* $(=2C_m^*)$ is smaller or the value of a/b is greater. For the limiting case of $C_t^* = C_m^* = 0$, however, U/U_0 resulting

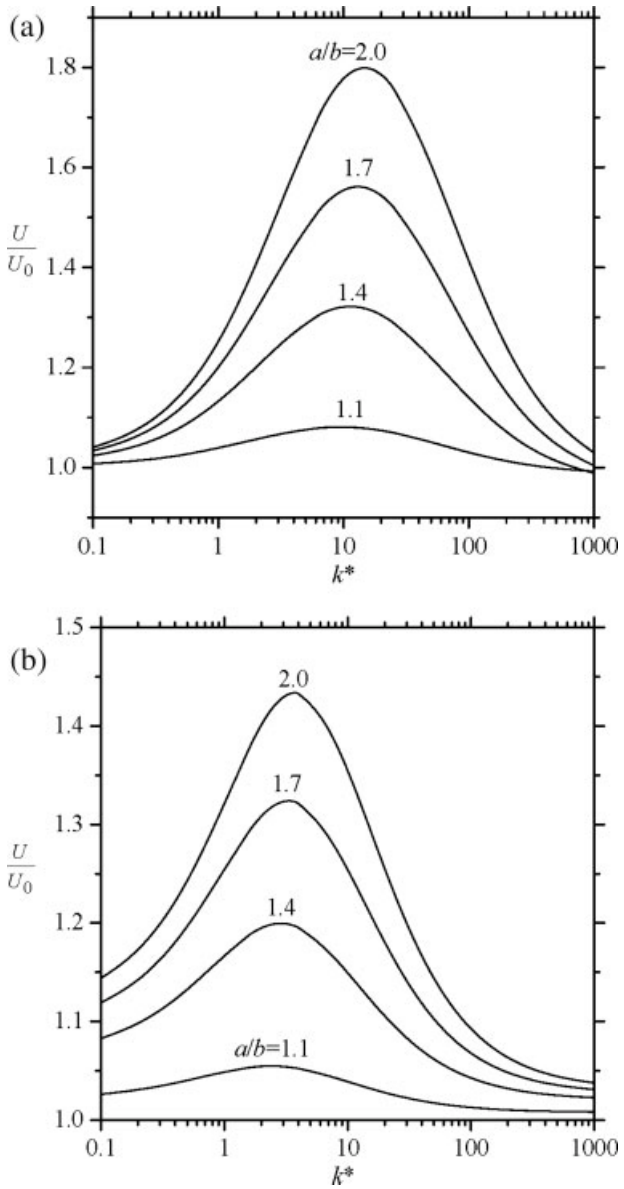

Figure 3. Plots of the normalized thermophoretic velocity U/U_0 of a prolate spheroidal particle along its axis of revolution vs. its relative conductivity k^* for various values of its aspect ratio a/b: (a) with $C_t^* = 2C_m^* = 0.02$; (b) with $C_t^* = 2C_m^* = 0.2$.

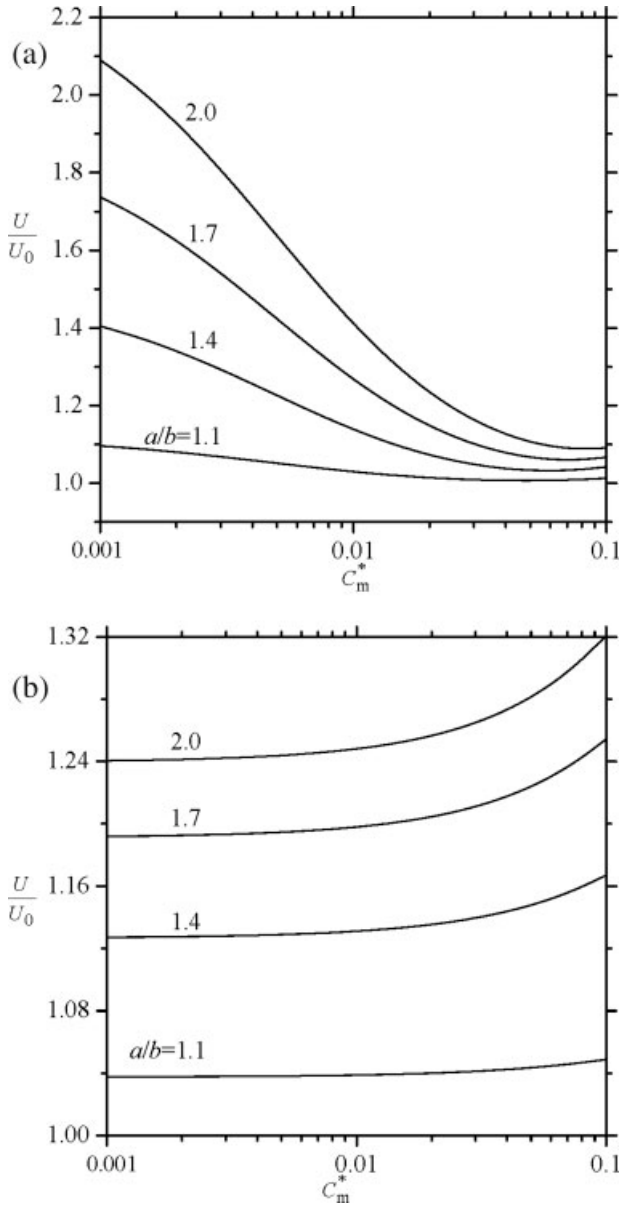

Figure 4. Plots of the normalized thermophoretic velocity U/U_0 of a prolate spheroidal particle with $C_t^* = 2C_m^*$ along its axis of revolution vs. C_m^* for various values of its aspect ratio a/b: (a) with $k^* = 100$; (b) with $k^* = 1$.

from Eq. 25 becomes a monotonically increasing function of k^*, keeping a/b as a constant. The reason for this behavior is that the thermophoretic mobility of the spheroid in the axial direction decreases with an increase in k^* and the sensitivity of this dependence increases with a decrease in a/b.[29] When C_t^* and C_m^* are small but finite and k^* is very large (e.g., $C_t^* = 2C_m^* = 0.02$ and $k^* = 1000$, as illustrated in Figure 3a), interestingly, U/U_0 may not be a monotonic function of a/b, and its value can be less than unity.

For fixed values of a/b and k^*, the value of U/U_0 decreases with an increase in C_t^* ($= 2C_m^*$) when C_t^* is small, reaches a minimum at some moderate value of C_t^*, and then increases with a further increase in C_t^*, when k^* is large (e.g., $k^* = 100$, as illustrated in Figure 4a), but increases monotonically with an increase in C_t^* when k^* is small (e.g., $k^* = 1$, as illustrated in Figure 4b). Because the effects of the four parameters k^*, C_t^*, C_m^*, and a/b on the thermophoretic velocity of a spheroid interact one another in a quite complicated manner (as indicated in Eq. 26), it would be very difficult to provide some physical analysis for the above observations from Figures 2–4.

If the particle velocity in Eq. 18 is disabled (i.e., $U = 0$ is set), then the force obtained from Eq. 23 can be taken as the thermophoretic force exerted on the spheroidal particle due to the imposed temperature gradient ∇T_∞. This force can be expressed as

$$F = 6\pi\eta b U_0 F^*, \tag{27}$$

where U_0 is the corresponding thermophoretic velocity of a spherical particle of radius b given by Eqs. 1 and 4 and F^* is the normalized magnitude of the thermophoretic force. The value of F^* also equals $f^* U/U_0$, where f^* is the dimensionless Stokes resistance coefficient of the spheroidal particle with frictional slip translating along its axis of revolution driven by a body force in the absence of the temperature gradient[33] and U is the thermophoretic velocity of the spheroidal particle obtained from Eq. 23 and the requirement $F = 0$.

Axisymmetric Thermophoresis of Oblate Particles

The axisymmetric thermophoresis of a general prolate particle was considered in a previous section and a set of spherical singularities must be distributed on a segment along the axis of symmetry inside the particle. In this section we consider the corresponding thermophoretic motion of a general oblate particle and the spherical singularities should be distributed on the fundamental surface within the particle. Because the oblate particle and the fluid motion are axisymmetric, the fundamental surface should be a circular disk S_d normal to the z-axis and with its center at the origin of the coordinate frame (the center of the particle).

Let Q be an arbitrary point on S_d which is expressed with the circular polar coordinates $\rho = \hat{\rho}$, $\phi = \hat{\phi}$, and $z = 0$. Then the temperature disturbance at another point P($\rho = \rho$, $\phi = 0$, $z = z$) generated by the spherical singularity at Q can be obtained using Eq. 7,

$$\begin{bmatrix} \hat{T} \\ \hat{T}_1 \end{bmatrix} = \begin{bmatrix} T_0 - E_\infty z \\ T_0 \end{bmatrix} + E_\infty \sum_{n=0}^{\infty} \begin{bmatrix} H_n L_{1n}(\rho^*, z) \\ \overline{H}_n L_{2n}(\rho^*, z) \end{bmatrix}, \tag{28}$$

where ρ^* is the distance from point Q to the projection of point P on the plane $z = 0$,

$$\rho^* = (\rho^2 + \hat{\rho}^2 - 2\rho\hat{\rho}\cos\hat{\phi})^{1/2}. \tag{29}$$

Similarly, the velocity disturbance at point P generated by the Sampson singularity at Q can also be obtained using Eq. 12

$$\hat{v}_\rho = \frac{\rho - \hat{\rho}\cos\hat{\phi}}{\rho^*}\sum_{n=2}^{\infty}[B_n A_{1n}(\rho^*, z) + D_n A_{2n}(\rho^*, z)], \quad (30a)$$

$$\hat{v}_\phi = \frac{\hat{\rho}\sin\hat{\phi}}{\rho^*}\sum_{n=2}^{\infty}[B_n A_{1n}(\rho^*, z) + D_n A_{2n}(\rho^*, z)], \quad (30b)$$

$$\hat{v}_z = \sum_{n=2}^{\infty}[B_n C_{1n}(\rho^*, z) + D_n C_{2n}(\rho^*, z)]. \quad (30c)$$

Because of the axisymmetry of the fluid motion, the singularities must be distributed uniformly on the circles in S_d with their centers at the origin of coordinates. Hence, the unknown density distribution coefficients H_n and $\overline{H}_n$ in Eq. 28 and B_n and D_n in Eq. 30 are functions of $\hat{\rho}$ only.

The total disturbance of the temperature field produced by the oblate particle can be approximated by the superposition of the individual disturbances in Eq. 28 induced by the whole set of singularities on the fundamental disk S_d. Thus, at an arbitrary location, we have

$$\begin{bmatrix} T \\ T_1 \end{bmatrix} = \begin{bmatrix} T_0 - E_\infty z \\ T_0 \end{bmatrix} + E_\infty \sum_{n=0}^{\infty}\int_0^{2\pi}\int_0^{R}\begin{bmatrix} H_n(\hat{\rho})L_{1n}(\rho^*, z) \\ \overline{H}_n(\hat{\rho})L_{2n}(\rho^*, z) \end{bmatrix}\hat{\rho}\, d\hat{\rho}\, d\hat{\phi}, \quad (31)$$

where R is the radius of the disk S_d. Equation 31 provides an exact solution for Eq. 5 that satisfies Eq. 6b, and the unknown density distribution functions $H_n(\hat{\rho})$ and $\overline{H}_n(\hat{\rho})$ must be determined from the remaining boundary conditions in Eq. 6a or 8 using the collocation method. In Eq. 8, the components of the temperature gradient can be calculated from Eq. 31 and expressed as

$$\begin{bmatrix} E_\rho \\ E_{1\rho} \end{bmatrix} = E_\infty \sum_{n=0}^{\infty}\int_0^{2\pi}\int_0^{R}\left\{\frac{\rho - \hat{\rho}\cos\hat{\phi}}{\rho^*}\begin{bmatrix} H_n(\hat{\rho})\delta_{1n}(\rho^*, z) \\ \overline{H}_n(\hat{\rho})\delta_{2n}(\rho^*, z) \end{bmatrix}\right\}\hat{\rho}\, d\hat{\rho}\, d\hat{\phi}, \quad (32a)$$

$$\begin{bmatrix} E_z \\ E_{1z} \end{bmatrix} = \begin{bmatrix} -E_\infty \\ 0 \end{bmatrix} + E_\infty \sum_{n=0}^{\infty}\int_0^{2\pi}\int_0^{R}\begin{bmatrix} H_n(\hat{\rho})\varepsilon_{1n}(\rho^*, z) \\ \overline{H}_n(\hat{\rho})\varepsilon_{2n}(\rho^*, z) \end{bmatrix}\hat{\rho}\, d\hat{\rho}\, d\hat{\phi}. \quad (32b)$$

The total disturbance of the flow field produced by the oblate particle can be approximated by the superposition of the individual disturbances in Eq. 30 induced by the whole set of Sampson singularities on the fundamental disk S_d. The expressions for the fluid velocity and stress components at an arbitrary location satisfying Eq. 11b analogous to Eqs. 31 and 32 for the temperature field have been obtained by Keh and Huang,[33] and the unknown density distribution functions $B_n(\hat{\rho})$ and $D_n(\hat{\rho})$ in these expressions must be determined from the remaining boundary conditions in Eq. 11a or 13 using the collocation method. With Eqs 15 and 31, the drag force exerted by the fluid on the oblate particle can be expressed as

$$F = 8\pi^2\eta\int_0^{R} D_2(\hat{\rho})\hat{\rho}\, d\hat{\rho}. \quad (33)$$

The density distribution functions $H_n(\hat{\rho})$, $\overline{H}_n(\hat{\rho})$, $B_n(\hat{\rho})$, and $D_n(\hat{\rho})$ in Eqs. 31 and 32 and related equations can be approximated to various orders of precision to satisfy the boundary conditions at the particle surface. Similar to the case of the thermophoresis of a prolate particle examined in a previous section, we consider the constant-distribution, linear-distribution, and quadratic-distribution approximations and their details incorporated with the boundary collocation technique to determine the thermophoretic velocity U of the particle are presented in the Supporting Information section. As the thermophoretic velocity of a sphere given by Eqs. 1 and 4, the value of U is proportional to the quantity $C_S\eta E_\infty/\rho_f T_0$ and dependent on the dimensionless parameters k^*, C_t^*, and C_m^* (in addition to the aspect ratios of the particle).

Solution for the Thermophoresis of an Oblate Spheroidal Particle

In a previous section, numerical solutions of the thermophoretic velocity of a prolate spheroid along its axis of revolution were presented. In this section the similar singularity method and collocation technique described in the previous section will be used to solve the corresponding velocity of an oblate spheroid. The shape of the oblate spheroid can still be represented by Eq. 24, but now with $b > a > 0$. In addition, the exact solution for the thermophoretic velocity of an oblate spheroid with no temperature jump and frictional slip ($C_t^* = C_m^* = 0$) along its axis of revolution can be expressed by[27–29]

$$U = C_s\frac{\eta E_\infty}{\rho_f T_0}\frac{\zeta[(\zeta^2+1)\cot^{-1}\zeta - \zeta]}{k^*(\zeta^2+1)(1-\zeta\cot^{-1}\zeta) + \zeta[(\zeta^2+1)\cot^{-1}\zeta - \zeta]}. \quad (34)$$

where $\zeta = a/c$ and $c = (b^2 - a^2)^{1/2}$, which is the radius of the focal circle of the oblate spheroid. In the limiting case of $a/b \to 1$ or $\zeta \to \infty$, Eq. 34 degenerates to Eq. 1 and 3 for a sphere.

The numerical solutions of the thermophoretic velocity U for the axisymmetric thermophoresis of an oblate spheroid

Table 3. Numerical Results of the Normalized Thermophoretic Velocity of an Oblate Spheroid with $C_t^* = 2C_m^*$ Along its Axis of Revolution for Various Values of the Aspect Ratio a/b and the Parameters k^* and C_m^*

a/b	k^*	C_m^*	$N_T = N_H$	M_T	M_H	U/U_0
0.9	100	0	4	10	9	0.8839
					10	0.8839
				11	11	0.8839
			Exact solution			0.8839
0.9	100	0.1	4	14	8	0.9842
					9	0.9844
					10	0.9844
				15	12	0.9844
			Approximate solution			0.9861
0.9	1	0.1	4	13	13	0.9448
					14	0.9450
					15	0.9450
				14	10	0.9450
			Approximate solution			0.9482
0.5	100	0	5	15	16	0.4533
					17	0.4533
				16	13	0.4533
			Exact solution			0.4533
0.5	100	0.1	5	23	14	0.8473
					15	0.8474
					16	0.8474
				24	14	0.8474
			Approximate solution			0.9303
0.5	1	0.1	5	19	12	0.6388
					13	0.6389
					14	0.6389
				20	11	0.6389
			Approximate solution			0.7412

Exact and approximate solutions are calculated from Eqs. 34 and 26, respectively.

with $C_t^* = 2C_m^*$ are presented in Table 3 for two representative cases of the aspect ratio a/b with various values of the thermal conductivity ratio k^* and the slip parameter C_m^*. Again, the magnitudes of this velocity are normalized by the corresponding thermophoretic velocity, U_0, of a spherical particle given by Eqs. 1 and 4. Either the linear (for $a/b = 0.9$) or the quadratic (for $a/b = 0.5$) density approximation of the singularity distribution is used to calculate the values of U and to show the convergence tests. The exact solution for the thermophoretic velocity of an oblate spheroid with no temperature jump and frictional slip along its axis of revolution given by Eq. 34 and the approximate solution for the axisymmetric thermophoretic velocity of a general spheroid whose shape deviates slightly from that of a sphere given by Eq. 26 with $\varepsilon = 1 - (a/b) > 0$ are also listed in Table 3 for comparison. Analogous to the case of a prolate spheroid considered in a previous section, the convergence behavior of the method of spherical singularities in general is satisfactory. The agreement between our results and the exact and approximate solutions is quite good. The errors of Eq. 26 are less than 0.4% for particles with $0.9 \leq a/b \leq 1$; but as expected, the accuracy of this approximate solution begins to deteriorate when the value of a/b becomes smaller.

The collocation solutions for the normalized thermophoretic velocity U/U_0 of an oblate spheroid with $C_t^* = 2C_m^*$ along its axis of revolution are plotted vs. the aspect ratio a/b, the conductivity ratio k^*, and the slip parameter C_m^* in Figures 5–7, respectively. For given values of k^*, C_t^*, and C_m^*, as expected, the value of U/U_0 in general decreases with a decrease in a/b, consistent with the trend predicted from Eq. 34 for the limiting case of $C_t^* = C_m^* = 0$. This behavior is understood because the fraction of the thermal slip of the fluid at the particle surface in the axial direction, which drives the movement of the particle, decreases with a decrease in a/b. Thus, the spherical approximation overestimates the axial thermophoretic mobility for oblate spheroids.

For fixed finite values of C_t^*, C_m^*, and a/b, the value of U/U_0 decreases with an increase in k^* when k^* is small, reaches a minimum at some moderate value of k^*, and then

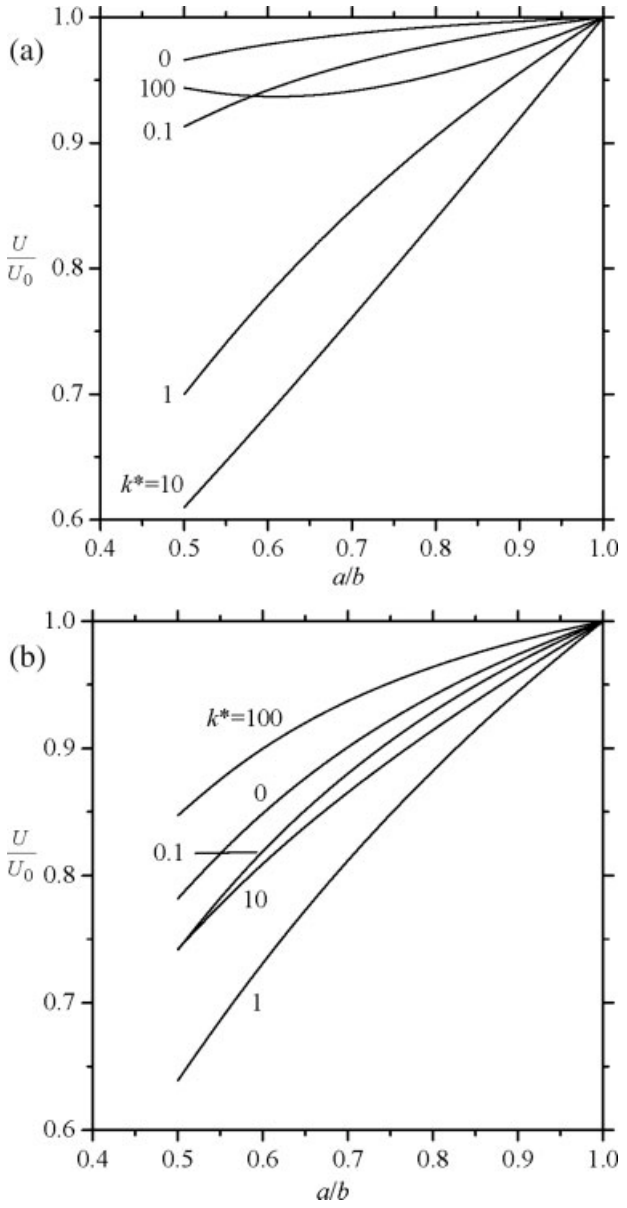

Figure 5. Plots of the normalized thermophoretic velocity U/U_0 of an oblate spheroidal particle along its axis of revolution vs. its aspect ratio a/b for various values of its relative conductivity k^*: (a) with $C_t^* = 2C_m^* = 0.02$; (b) with $C_t^* = 2C_m^* = 0.2$.

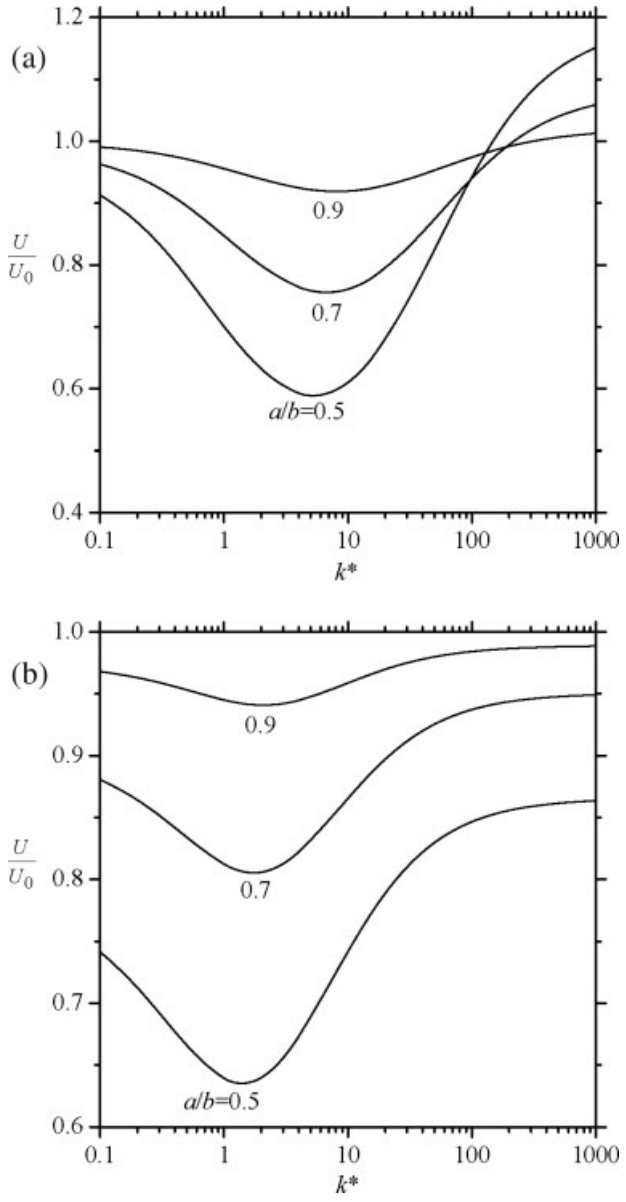

Figure 6. Plots of the normalized thermophoretic velocity U/U_0 of an oblate spheroidal particle along its axis of revolution vs. its relative conductivity k^* for various values of its aspect ratio a/b: (a) with $C_t^* = 2C_m^* = 0.02$; (b) with $C_t^* = 2C_m^* = 0.2$.

increases with a further increase in k^*. This minimum occurs at a higher value of k^* if the value of C_t^* $(=2C_m^*)$ is smaller or the value of a/b is greater. For the limiting case of $C_t^* = C_m^* = 0$, however, U/U_0 resulting from Eq. 34 becomes a monotonically decreasing function of k^*, keeping a/b unchanged. Again, the reason for this behavior is that the thermophoretic mobility of the spheroid in the axial direction decreases with an increase in k^* and the sensitivity of this dependence increases with a decrease in a/b.

When C_t^* and C_m^* are small but finite and k^* is large (e.g., $C_t^* = 2C_m^* = 0.02$ and $k^* \geq 100$, as illustrated in Figures 5a and 6a), interestingly, U/U_0 may not be a monotonic function of a/b, and its value can be greater than unity. For specified values of a/b and k^*, the value of U/U_0 increases with an increase in C_t^* $(=2C_m^*)$ when C_t^* is small, reaches a maximum at some moderate value of C_t^*, and then decreases with a further increase in C_t^*, when k^* is large (e.g., $k^* = 100$, as illustrated in Figure 7a), but decreases monotonically with an increase in C_t^* when k^* is small (e.g., $k^* = 1$, as illustrated in Figure 7b). Because the effects of the parameters k^*, C_t^*, C_m^* and a/b on the thermophoretic velocity of a spheroid interact one another in a quite complicated manner, it would be very

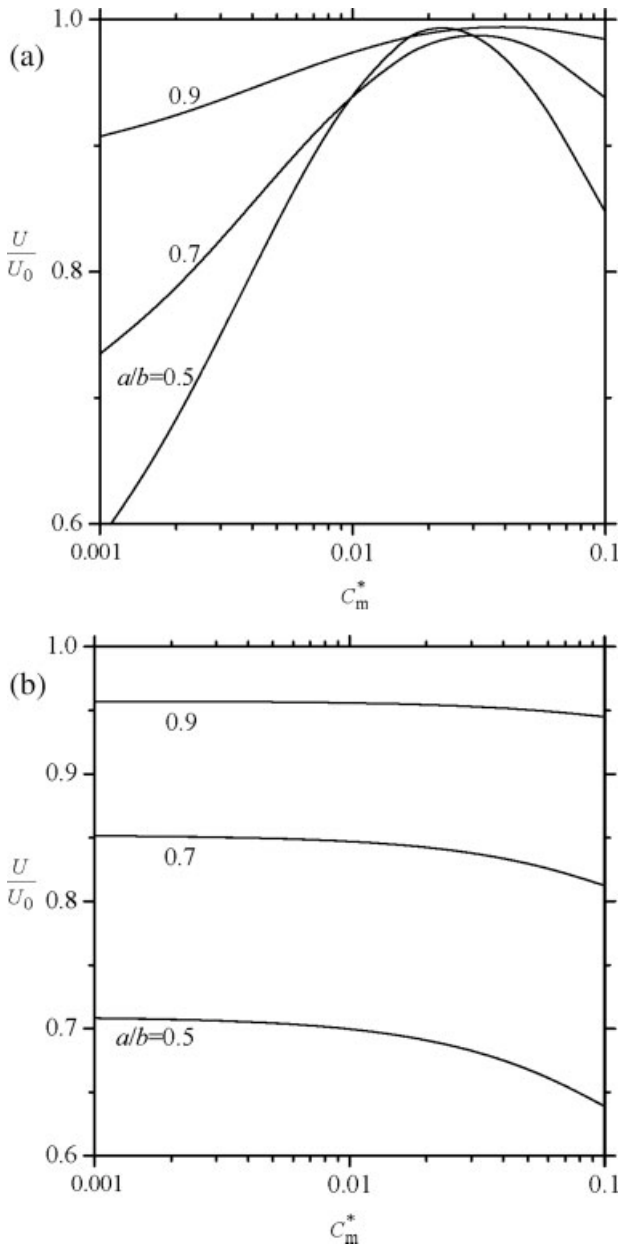

Figure 7. Plots of the normalized thermophoretic velocity U/U_0 of an oblate spheroidal particle with $C_t^* = 2C_m^*$ along its axis of revolution vs. C_m^* for various values of its aspect ratio a/b: (a) with $k^* = 100$; (b) with $k^* = 1$.

difficult to provide the physical analysis for some observations from Figures 5–7.

The thermophoretic force exerted on the oblate spheroidal particle due to the applied temperature gradient ∇T_∞ (the force obtained from Eq. 33 when $U = 0$ is set) can also be expressed as Eq. 27. The value of F^* still equals $f^* U/U_0$, but now U is the thermophoretic velocity of the oblate spheroidal particle obtained from Eq. 33 and the constraint $F = 0$.

Concluding Remarks

In this work the thermophoresis of a general axisymmetric particle with a temperature jump, a thermal slip, and a frictional slip at its surface in a viscous fluid (e. g., a slightly rarefied gas) along its axis of revolution has been analyzed by the use of the method of internal singularity distributions combined with the boundary-collocation technique. For the case of the axisymmetric thermophoresis of a prolate particle, a truncated set of spherical singularities is distributed along the axis; whereas for the case of an oblate particle, the singularities are placed on the fundamental disk of the particle. The results for the thermophoretic velocity of the particle indicate that the solution procedure converges rapidly and accurate solutions can be obtained for various cases of the physical and surface properties of the particle-fluid system and of the particle shape. It is found that the normalized thermophoretic velocity of a spheroid, prolate or oblate, along its axis of revolution in general increases with an increase in its axial-to-radial aspect ratio a/b; the exceptions may occur when the relative jump/slip coefficients at the particle surface, C_t^* and C_m^*, are small but finite and the relative thermal conductivity of the particle, k^*, is large. For most practical cases of a spheroid with a fixed a/b, the thermophoretic mobility of the particle is not a monotonic function of k^*, C_t^* and C_m^*. The results indicate that the shape (e.g., prolate or oblate) and the relative physical and surface properties of a nonspherical particle can have significant effects on its thermophoretic behavior.

It is worth repeating that our results are obtained on the basis of a continuum model for the gas phase with a slip-flow boundary condition at the particle surface. For a perfect gas, the kinetic theory predicts that the mean free path of gas molecules is inversely proportional to the pressure. As examples, the mean free path of air molecules at 25 °C is about 67 nm at 1 atm and is about 51 μm at 1 torr.[41] Therefore, our results obtained with the assumption of small Knudsen number can be used for a broad range of particle sizes (about 0.5 μm or larger) around atmospheric pressure but is only applicable for relatively large particles (about 0.1 mm or larger) at low pressures.

Although the numerical solutions were presented in the previous sections only for the thermophoresis of a sphere, a prolate spheroid and an oblate spheroid, the combined analytical and numerical technique utilized in this work can easily provide the calculations for the thermophoretic velocity of an axisymmetric particle of other shapes, such as a prolate or oblate Cassini oval.[32] Moreover, the method of axisymmetric singularity distribution can also be utilized to investigate some three-dimensional (asymmetric) thermal and hydrodynamic fields induced by the thermophoretic motion of an aerosol particle of revolution, as in an approach for the translation of a prolate spheroid in an arbitrary direction with respect to its axis of symmetry in an unbounded fluid.[42]

Acknowledgments

This research was partly supported by the National Science Council of the Republic of China.

Notation

a = half-length of a spheroid along its axis of revolution, m
b = maximum cross-sectional radius of a spheroid, m
B_n, D_n = coefficients in Eq. 12 for the fluid velocity field, $m^{n+2} \cdot s^{-1}$, $m^n \cdot s^{-1}$
C_m = dimensionless coefficient accounting for the frictional slip
$C_m^* = C_m l/b$
C_s = dimensionless coefficient accounting for the thermal slip
C_t = dimensionless coefficient accounting for the temperature jump
$C_t^* = C_t l/b$
$E_\infty = |\nabla T_\infty|$, K m^{-1}
E_ρ, E_z = ρ and z components of temperature gradient outside the particle, K m^{-1}
$E_{1\rho}, E_{1z}$ = ρ and z components of temperature gradient inside the particle, K m^{-1}
F = hydrodynamic drag force on the particle, N
$G_n^{-1/2}$ = Gegenbauer polynomial of the first kind of order n and degree $-1/2$
$H_n, \overline{H}_n$ = coefficients in Eq. 7 for the temperature field, m^{n+2}
k = thermal conductivity of the fluid, W m^{-1} K^{-1}
k_1 = thermal conductivity of the particle, W m^{-1} K^{-1}
$k^* = = k_1/k$
l = mean free path of the gas molecules, m
M = thermophoretic mobility defined by Eq. 1, m^2 s^{-1} K^{-1}
M_T, N_T, M_H, N_H = numbers of collocation points on the particle surface
$\mathbf{n}$ = unit normal vector at particle surface pointing into the fluid
n_ρ, n_z = ρ and z components of $\mathbf{n}$
P_n = Legendre function of order n
r = radial spherical coordinate, m
S_p = particle surface
T = temperature field in the fluid, K
T_1 = temperature field inside the particle, K
T_0 = mean fluid temperature in the vicinity of the particle, K
T_∞ = prescribed temperature field defined by Eq. 6b, K
U = particle velocity, m s^{-1}
U_0 = velocity of a spherical particle, m s^{-1}
$\mathbf{v}$ = velocity field of the fluid, m s^{-1}
v_ρ, v_z = components of $\mathbf{v}$ in cylindrical coordinates, m s^{-1}
z = axial cylindrical coordinate, m

Greek letters

η = viscosity of the fluid, kg m^{-1} s^{-1}
ϕ = angular cylindrical coordinate
ρ = radial cylindrical coordinate, m
ρ_f = density of the fluid, kg m^{-3}

Literature Cited

1. Waldmann L, Schmitt KH. Thermophoresis and diffusiophoresis of aerosols. In: Davies CN, editor. *Aerosol Science*. New York: Academic Press, 1966:137–162.
2. Friedlander SK. *Smoke, Dust and Haze*. New York: Wiley, 1977.
3. Batchelor GK, Shen C. Thermophoretic deposition of particles in gas flowing over cold surfaces. *J Colloid Interface Sci*. 1985;107:21–37.
4. Montassier N, Boulaud D, Renoux A. Experimental study of thermophoretic particle deposition in laminar tube flow. *J Aerosol Sci*. 1991;22:677–687.

5. Messerer A, Niessner R, Poschl U. Miniature pipe bundle heat exchanger for thermophoretic deposition of ultrafine soot aerosol particles at high flow velocities. *Aerosol Sci Technol*. 2004;38:456–466.
6. Weinberg MC. Thermophoretic efficiency in modified chemical vapor deposition process. *J Am Ceram Soc*. 1982;65:81–87.
7. Balsara NP, Subramanian RS. The influence of buoyancy on thermophoretic deposition of aerosol particles in a horizontal tube. *J Colloid Interface Sci*. 1987;118:3–14.
8. Ye Y, Pui DYH, Liu BYH, Opiolka S, Blumhorst S, Fissan H. Thermophoretic effect of particle deposition on a free standing semiconductor wafer in a clean room. *J Aerosol Sci*. 1991;22:63–72.
9. Williams MMR, Loyalka SK. *Aerosol Science: Theory and Practice, with Special Applications to the Nuclear Industry*. Oxford: Pergamon Press, 1991.
10. Kennard EH. *Kinetic Theory of Gases*. New York: McGraw-Hill, 1938.
11. Maxwell JC. On stresses in rarified gases arising from inequalities of temperature. *Philos. Trans. R. Soc*. 1879;170:231–256.
12. Epstein PS. Zur theorie des radiometers. *Z Phys*. 1929;54:537–563.
13. Brock JR. On the theory of thermal forces acting on aerosol particles. *J Colloid Sci*. 1962;17:768–780.
14. Schadt CF, Cadle RD. Thermal forces on aerosol particles. *J Phys Chem*. 1961;65:1689–1694.
15. Li W, Davis EJ. Measurement of the thermophoretic force by electrodynamic levitation: microspheres in air. *J Aerosol Sci*. 1995;26:1063–1083.
16. Derjaguin BV, Storozhilova AI, Rabinovich YaI. Experimental verification of the theory of thermophoresis of aerosol particles. *J Colloid Interface Sci*. 1966;21:35–58.
17. Derjaguin BV, Rabinovich YaI, Storozhilova AI, Shcherbina GI. Measurement of the coefficient of thermal slip of gases and the thermophoresis velocity of large-size aerosol particles. *J Colloid Interface Sci*. 1976;57:451–461.
18. Talbot L, Cheng RK, Schefer RW, Willis DR. Thermophoresis of particles in heated boundary layer. *J Fluid Mech*. 1980;101:737–758.
19. Cercignani C. *Rarefied Gas Dynamics: from Basic Concepts to Actual Calculations*. Cambridge: Cambridge University Press, 2000.
20. Sone Y. *Kinetic Theory and Fluid Dynamics*. Boston: Birkhauser, 2002.
21. Sharipov F, Kalempa D. Velocity slip and temperature jump coefficients for gaseous mixtures. II. Thermal slip coefficient. *Phys Fluids*. 2004;16:759–764.
22. McCormick NJ. Gas-surface accommodation coefficients from viscous slip and temperature jump coefficients. *Phys. Fluids* 2005; 17:107104-1-8.
23. Dahneke BE. Slip correction factors for nonspherical bodies: introduction and continuum flow. *J Aerosol Sci*. 1973;4:139–145.
24. Laucks ML, Roll G, Schweiger G, Davis EJ. Physical and chemical (Raman) characterization of bioaerosols: pollen. *J Aerosol Sci*. 2000;31:307–319.
25. Reed LD. *A continuum slip flow analysis of steady and transient thermophoresis*. M.S. thesis, University of Illinois, Urbana-Champaign, Illinois, 1971.
26. Keh HJ, Tu HJ. Thermophoresis and photophoresis of cylindrical particles. *Colloids Surf A*. 2001;176:213–223.
27. Leong KH. Thermophoresis and diffusiophoresis of large aerosol particles of different shapes. *J Aerosol Sci*. 1984;15:511–517.
28. Williams MMR. Thermophoretic forces acting on a spheroid. *J Phys D*. 1986;19:1631–1642.
29. Keh HJ, Ou CL. Thermophoresis of aerosol spheroids. *Aerosol Sci Technol*. 2004;38:675–684.
30. Senchenko S, Keh HJ. Thermophoresis of a slightly deformed aerosol sphere. *Phys Fluids*. 2007;19:033102-1-12.
31. Lienhard JH. *A Heat Transfer Textbook*, 2nd ed. Englewood Cliffs, New Jersey: Prentice-Hall, 1987.
32. Keh HJ, Tseng CH. Slow motion of an arbitrary axisymmetric body along its axis of revolution and normal to a plane surface. *Int J Multiphase Flow*. 1994;20:185–210.
33. Keh HJ, Huang CH. Slow motion of axisymmetric slip particles along their axes of revolution. *Int J Eng Sci*. 2004;42:1621–1644.
34. Keh HJ, Chen SH. Particle interactions in thermophoresis. *Chem Eng Sci*. 1995;50:3395–3407.
35. Sampson RA. On Stokes's current function. *Philos Trans R Soc A* 1891;182:449–518.
36. Happel J, Brenner H. *Low Reynolds Number Hydrodynamics*. Dordrecht, The Netherlands: Nijhoff, 1983.
37. O'Brien V. Form factors for deformed spheroids in Stokes flow. *AIChE J*. 1968;14:870–875.
38. Gluckman MJ, Pfeffer R, Weinbaum S. A new technique for treating multi-particle slow viscous flow: axisymmetric flow past spheres and spheroids. *J Fluid Mech*. 1971;50:705–740.
39. Ganatos P, Weinbaum S, Pfeffer R. A strong interaction theory for the creeping motion of a sphere between plane parallel boundaries. I. Perpendicular motion. *J Fluid Mech*. 1980;99:739–753.
40. Keh HJ, Chang YC. Thermophoresis of an aerosol sphere perpendicular to two plane wells. *AIChE J*. 2006;52:1690–1704.
41. Shoemaker DP, Garland CW, Steinfeld JI, Nibler JW. *Experiments in Physical Chemistry*, 4th ed. New York: McGraw-Hill, 1981.
42. Lin S, Wu W. The semi-analytic semi-numerical method to treat the three-dimension Stokes flow. *Acta Aerodyn Sin*. 1986;4:140–149 (in Chinese).

Manuscript received May 24, 2007, revision received Feb. 4, 2008, and final revison received July 17, 2008.